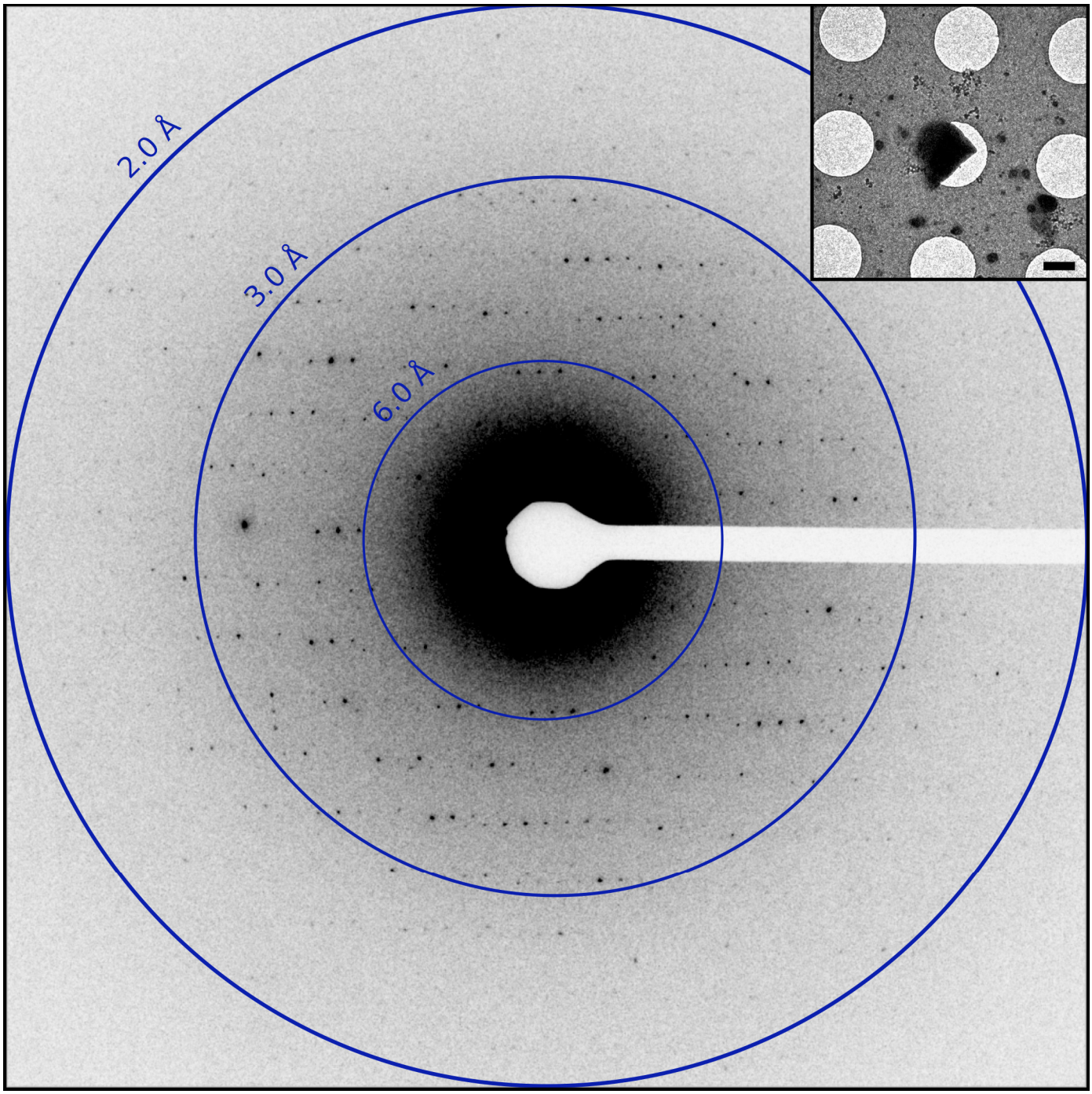

Supplementary Figure 1

Resolution of lysozyme microcrystals collected by continuous rotation.

Lysozyme microcrystals were visualized by cryo-EM prior to data collection and a representative crystal is shown (inset, scale bar represents 1 μm). Well diffracting crystals were typically on the order of 2 μm x 2μm x 0.5 μm in size. The crystal shown is a wedge that measured as 0.5 μm thick at the center and 0.15 μm thick at the edges. A representative diffraction pattern from a lysozyme microcrystal collected under continuous rotation. This individual frame was collected over 4 s at a dose of ~0.01 $e^-/Å^2/s$ and a rotation rate of 0.09° s^{-1}. The diffraction pattern shows visible reflections extending to ~ 2 Å resolution and beyond. The contrast of this image was enhanced in Fiji[25] to enable spot visualization for this figure.

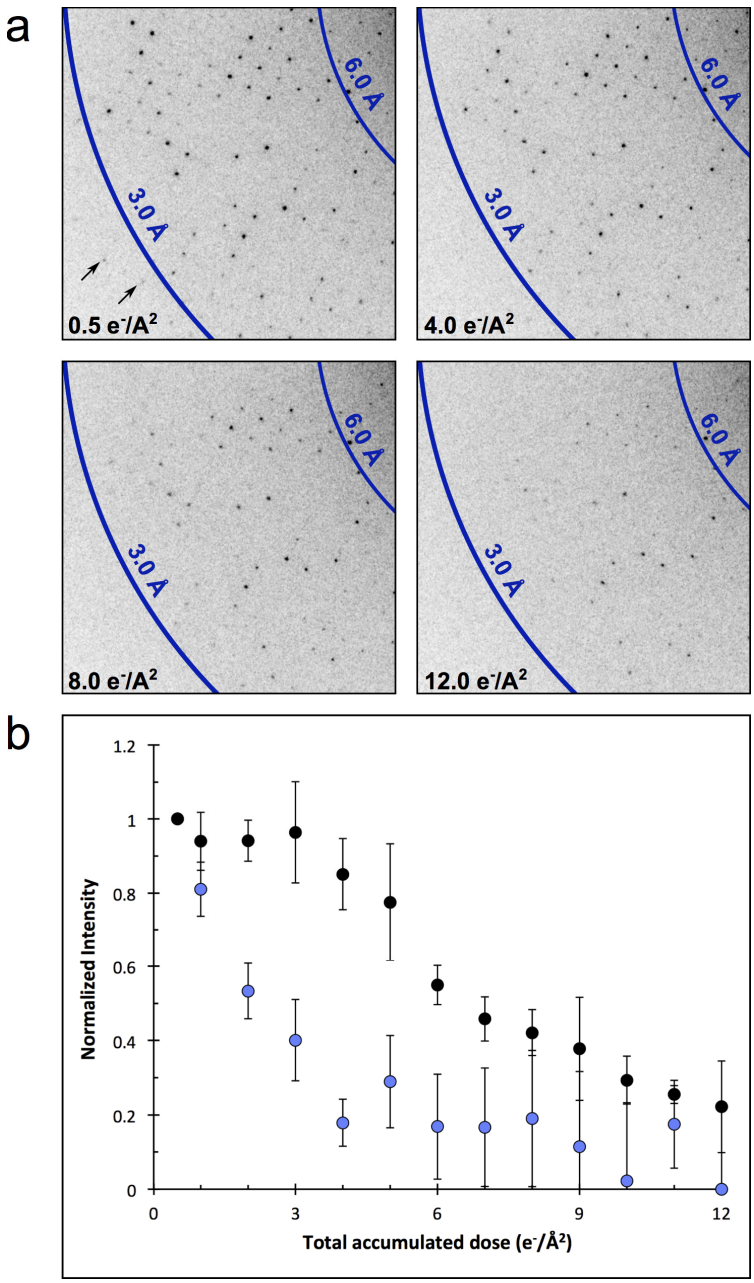

Supplementary Figure 2

Radiation damage assessment of continuously exposed microcrystals.

(a) A single crystal was exposed continuously for 120 frames for a final accumulated dose of 12.0 e^-/A^2 (0.1 e^-/A^2 per frame). A representative region from diffraction patterns originating from the same crystal in the same orientation is shown as a function of accumulated dose. It can be seen qualitatively that the intensities of the reflections decrease as dose is accumulated, especially at higher resolutions (see arrows in top left panel), and this effect becomes more severe for all reflections at the higher dosages (8.0 e^-/A^2 and 12.0 e^-/A^2). (b) In order to more quantitatively investigate the negative effects of radiation damage, intensities in the resolution bins of 2 - 3 Å (2 randomly chosen reflections) as well as 3 - 6 Å (7 randomly chosen reflections) were selected and their normalized intensity as a function of accumulated dose was analyzed. It was found that the higher resolution reflections suffer relatively early (~2 $e^-/Å^2$ of total accumulated dose, blue), whereas the intensities between 3 Å and 6 Å do not decrease drastically until approximately 5 to 6 $e^-/Å^2$ of total accumulated dose (black). Error bars represent standard error of the mean.

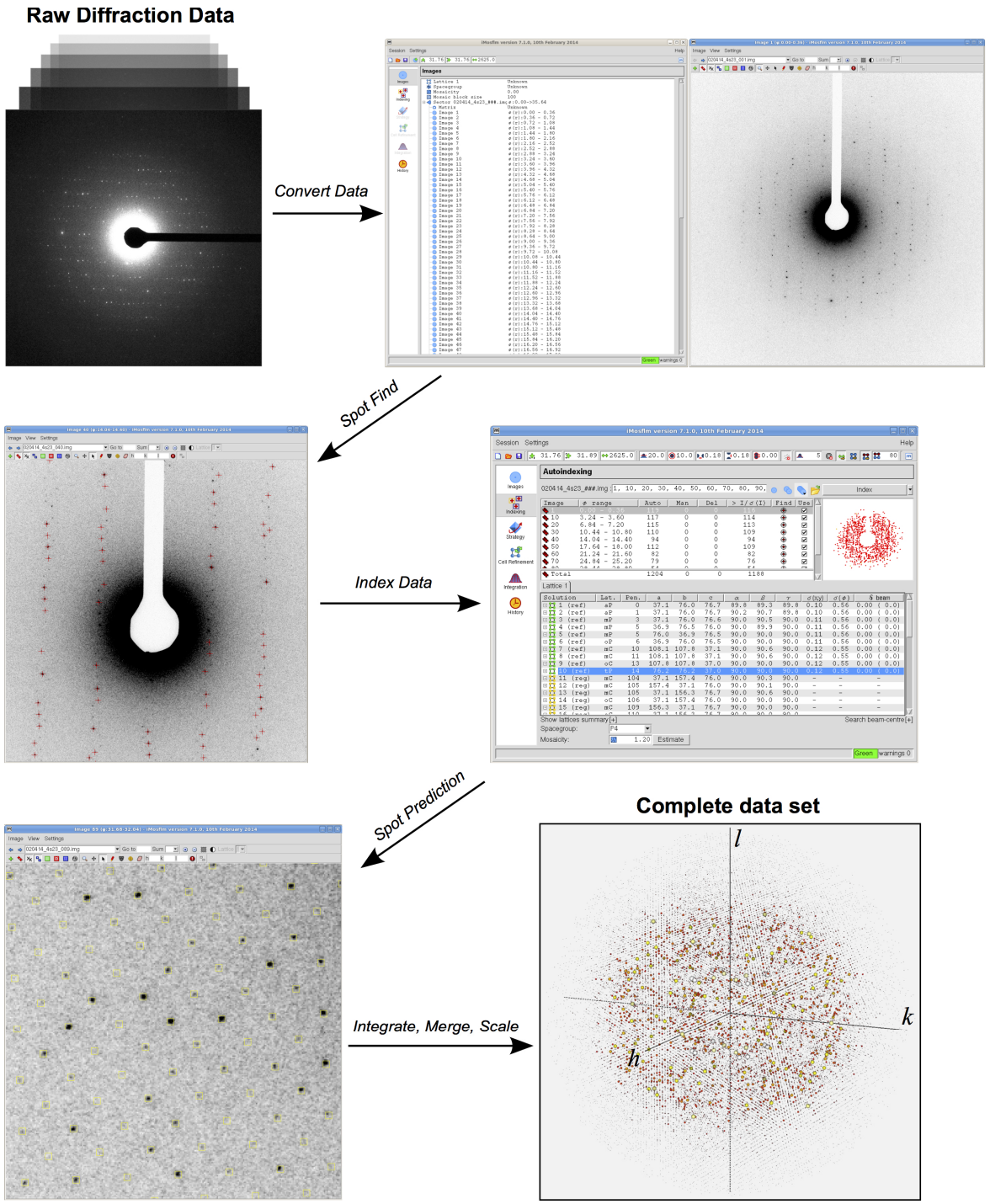

Supplementary Figure 3

Process flow from raw data to completely processed data set using MOSFLM.

The raw data collected on the TEM is first converted to a file compatible with MOSFLM by an in-house script. MOSFLM then uses automated spot finding to determine the position of the reflections on the images. Following spot finding MOSFLM uses the relative positions of each reflection to determine crystal lattice parameters and the crystals orientation. This then allows the location of each reflection within the data set to be predicted, properly indexed, and integrated. After merging and scaling, process of converting the many raw diffraction patterns into one reflection file is complete.

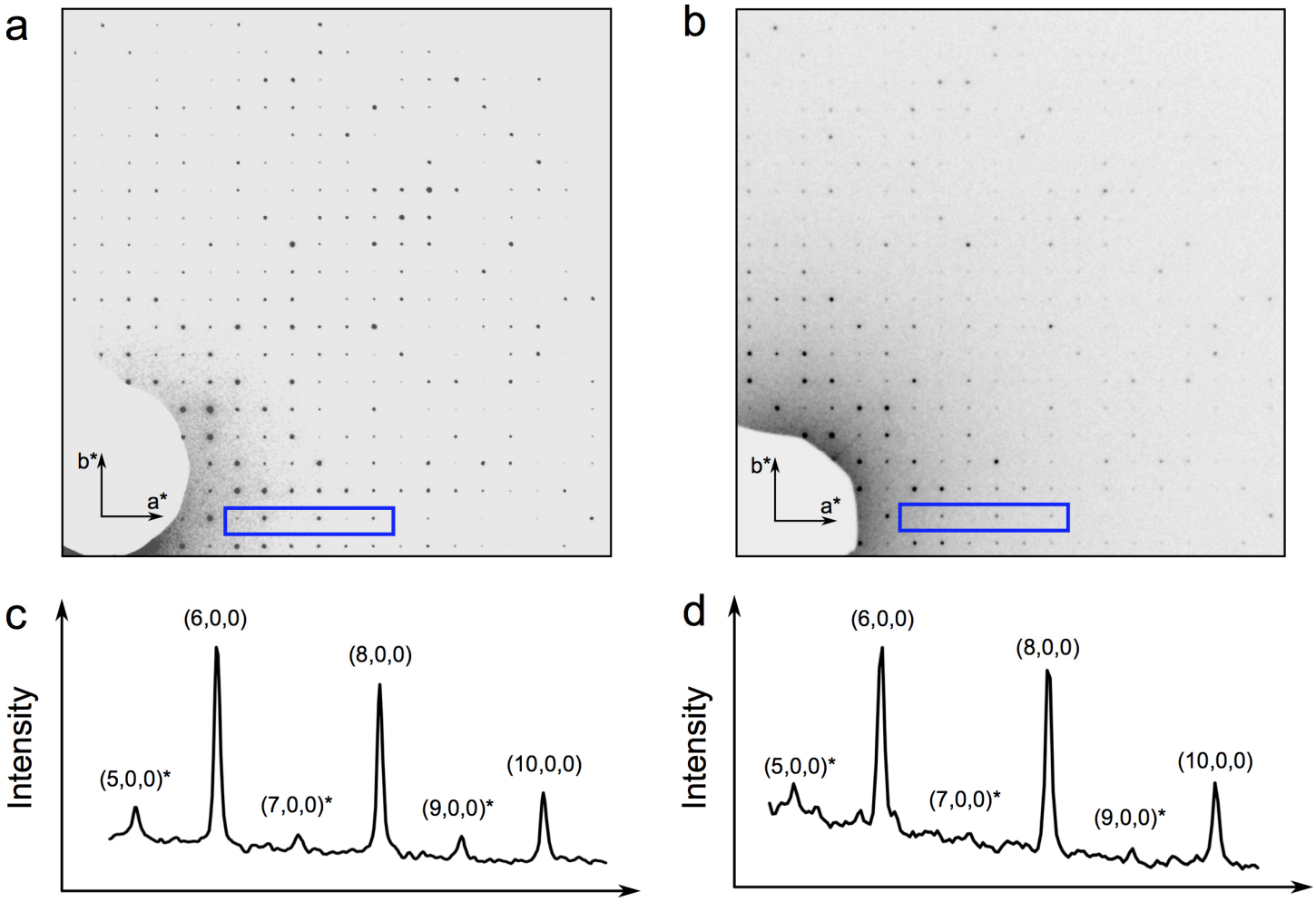

Supplementary Figure 4

Continuous rotation reduces dynamical scattering.

(a-b) Diffraction patterns near the (001) major planes of lysozyme were used to assess the level of dynamic scattering by looking at the systematic absences along the a* axis for both still diffraction data (a) and continuously rotated diffraction data (b). The data from (a) and (b) come from two different crystals. (c-d) The intensity of reflections along a* was quantified and plotted for the still diffraction and continuously rotated diffraction patterns (the portion of the diffraction patterns indicated by the box inset). The plot from still diffraction (c) clearly show small but significant levels of intensity coming from dynamic scattering for reflections (2n+1,0,0), which are forbidden in $P4_32_12$ symmetry. The intensities of these forbidden reflections are greatly reduced when continuous rotation is used (d).

SUPPLEMENTARY INFORMATION

Supplementary Results

Radiation damage assessment

Previously, we assessed the radiation damage for the collection of still data sets, where the crystal undergoes pulses of exposure followed by a rest period as the crystal is tilted[4]. When collecting still data sets, the dose where reflection intensities from a single lysozyme microcrystal began to deteriorate was ~ 9 $e^-/Å^2$. This allowed us to collect up to 90 frames at the set dose rate of 0.01 $e^-/Å^2/s$ with a 10 s exposure per frame.

In the continuous rotation method, the crystal is continuously exposed to the electron beam without rest periods, therefore, it was important to characterize the radiation damage to determine how long the crystal could be exposed before radiation damage became too severe and the crystal was destroyed. Again, we used lysozyme as a model microcrystal and examined the decrease in reflection intensities as the electron beam constantly bombarded the sample during a continuous exposure (Supplementary Video 1). The microcrystal was oscillated between -1° and 1° to collect full intensities and to account for beam-induced crystal rocking that could affect the recorded intensities. The microcrystal was subjected to 120 exposures, each at a total dose of 0.1 $e^-/Å^2$ without pausing between exposures, and the intensities as a function of dose were measured for randomly chosen reflections in the ranges of 2-3 Å and 3-6 Å (Supplemental Fig. 2). We found that the crystal experiences significant radiation damage, especially beyond a total dose of ~6 $e^-/Å^2$ where the measured intensities dropped below ~50% of their original value. The higher resolution reflections deteriorate at a higher rate than those at lower resolution. Reflections in the 2-3Å resolution range vanished very quickly, within a total dose of only ~2$e^-/Å^2$ leading to a 50% reduction in measured intensity.

These results are significantly different than for the still data set[4]. It is possible that with pulses followed by rest periods of up to 10 s, the free radicals[21] and hydrogen gas[22] generated during the exposure have time to diffuse from the

microcrystal during the rest period, before they can accumulate to high concentrations and cause substantial damage. However, with a continuous exposure the accumulation of free radicals or hydrogen gas could exceed the diffusion rate, leading to higher concentration of damaging species and increased levels of damage. It is also possible that increased sample heating[23] caused by the incident beam during the continuous exposure is a significant factor contributing to the observed rapid decay of the crystal lattice during the continuous exposure. This suggests that lowering the intensity of the electron beam and recording the diffraction data over longer times may decrease the effects of beam-induced damage, however this is currently not possible with the current experimental set up. Future analysis and optimization should help clarify the effects of radiation damage during continuous rotation. While these data indicate there is more radiation damage for continually exposed crystals, our hypothesis was that the improvement in overall data quality by continuous rotation justifies the higher levels of radiation damage. We therefore set the limit for continuously rotated data sets to < 5 $e^-/Å^2$ where the damaging effects of the electron beam appear tolerable.

Using MOSFLM with continuous rotation data

The images from the TVIPS CMOS detector were converted to the Super Marty View (SMV) image format, which is a format recognized by MOSFLM. Based on the distribution of pixel values in these images, the ADC offset parameter was set to zero. The MOSFLM gain parameter was set to 2.0, a value derived by observing the variation in background regions around diffraction spots and adjusting the gain so that this matched the variation expected from Poisson statistics. The background levels in the images at high resolution were very low and pixels with a value of zero were not uncommon. To avoid rejecting reflections that included pixels with a value of zero, the "Null pixel threshold" parameter was set to -1 (the default value is zero).

Correct indexing was not possible for a single MicroED pattern, while this is possible for most X-ray diffraction images. This because the Ewald sphere in our experiments has a very limited curvature for the wavelength used (0.025 Å),

Nature Methods: doi:10.1038/nmeth.3043

resulting in very limited information about the reciprocal space parameters along the beam direction. In practice it was found that several images spaced over a tilt range of at least 20° were required, and the most robust indexing results were obtained using 6 images equally spaced in phi, covering a total rotation range of 35°.

The cell parameters from indexing were used for integration, without any further refinement. When integrating the images, the detector tilt and twist parameters (describing rotations of the detector plane about axes parallel and normal to the rotation axis respectively) were not well defined and were fixed at zero. This is due to the relatively small size of the detector (64 x 64 mm) and the lack of strong reflections at higher resolution.

The crystal mosaicity required particular attention. Because of the way in which the CMOS detector is read out while the crystal is continuously rotating, the effective rotation range of an image is continually shifted across the image (see explanation below). At present there is no way of allowing for this in the MOSFLM software (although the necessary changes are now being introduced). To avoid missing reflections that are present on an image, but would not be predicted to be present based on the nominal start and end phi values for that image, the crystal mosaicity was set to an artificially high value of 2° and the mosaic block size was set to 5 microns. This resulted in significant over-prediction (as judged by the width of individual reflection lunes) but successfully predicted all the spots present on the image. Smaller values for the mosaic spread resulted in a significant deterioration in data quality as judged by the merging R-factor. The effect of the high mosaicity will be to include more background along with the true Bragg intensity when integrating any particular reflection, because a reflection will be predicted to be present on more images than it actually is. This will result in a loss in data quality that will be most apparent for the weak, high-resolution reflections. The mosaic block size parameter is almost certainly an imperfect way of modelling what is actually happening in the crystal, but it is certainly much better than making no correction at all. That is why the absolute value of the mosaic block size that gives the best prediction cannot be directly translated into the physical mosaic block size of the crystal. The value is adjusted heuristically to get the best prediction of what is observed in the diffraction pattern.

Nature Methods: doi:10.1038/nmeth.3043

Therefore, the mosaic block model is not a perfect model of the physical reality and the absolute value cannot be taken too literally, but the advantage of using this model in terms of the quality of the resulting data (especially Rmerge at low resolution) is very clear (Supplemental Table 1).

The increased mosaicity is necessary because of the "rolling shutter" mode of the detector readout. In this mode, each line of pixels in the image (4096 x 4096 pixels) is read out sequentially, line by line, with a readout time of ~100 μs during which time that line of pixels is inactive (but the remainder of the detector is still active). Immediately following readout, the line of pixels becomes active again. It takes ~400 ms to read out the entire detector, and during this time, the crystal is rotating continuously. As a result, the rotation angle corresponding to the beginning of the exposure varies across the detector. The rotation angle corresponding to the end of the exposure for each line (i.e. immediately before that line is read out) varies in the same way. Thus, for all lines making up the image, the total rotation angle per exposure is the same (0.36° in these experiments), but the starting (and ending) rotation angle differs across the image. This is quite different to the readout for typical CCD or image plate detectors used in X-ray diffraction, where the shutter is closed and the crystal rotation is stopped while the entire image is read out. Correctly allowing for the mode of the detector readout and further optimization of data collection parameters and equipment (e.g. per frame rotation range and faster read-out times from the detector) should therefore extend the resolution of the analyzed diffraction data beyond that reported here and should allow us to reach the recorded resolution limit of ~1.9Å of our data.

Nature Methods: doi:10.1038/nmeth.3043

Supplementary Table 1. Data collection and refinement statistics

Data Collection

Excitation voltage	200kV
Electron Source	Field Emission Gun
Wavelength (Å)	0.025
Total dose per crystal ($e^-/Å^2$)	~4.5
Frame rate (s/frame)	4
Rotation rate (°/s)	0.09
Total Angular range per crystal (°)	~44

Merging Statistics	2 total crystals	Single crystal
Space group	$P4_32_12$	$P4_32_12$
Unit cell dimensions		
a, b, c (Å)	76.0 Å, 76.0 Å, 37.2 Å	75.9 Å, 75.9 Å, 36.9 Å
$\alpha=\beta=\gamma$	90°	90°
Resolution	11.4 – 2.5 Å	11.2 – 2.5 Å
Total reflections	19181	10723
R_{merge} (%)[c]	13.9 (29.9)[a]	15.5 (29.2)[a]
Total Unique Reflections	3964	3116
Multiplicity	4.8 (4.9)[a]	3.4 (3.2)[a]
Completeness (%)	97.2 (90.2)[a]	80.1 (80.1)[a]
Mean (I/σ(I))	11.8 (6.0)[a]	8.7 (4.7)[a]

Data Refinement

Reflections in working set	3772	2973
Reflections in test set	180	143
R_{work}/R_{free} (%)	22.0/25.5	21.3/25.3
RMSD Bonds	0.003 Å	0.003 Å
RMSD Angles	0.60°	0.60°
Ramachandran (%)[b]		
(Favored, allowed, outlier)	97.9; 2.1; 0	96.0; 4.0; 0

[a] Values for highest resolution shell of 2.6 Å – 2.5 Å

[b] Statistics given by MolProbity[24]

[c] $R_{\text{merge}} = \frac{\sum_i \sum_j |I_{i,j} - \langle I_i \rangle|}{\sum_i \sum_j I_{i,j}}$; where $I_{i,j}$ is the integrated intensity for the j^{th} observation of the unique reflection i and $\langle I_i \rangle$ is the weighted mean intensity for reflection i.

Nature Methods: doi:10.1038/nmeth.3043

SUPPLEMENTARY REFERENCES

21. Henderson, R. *P Roy Soc B-Biol Sci* **241**, 6-8 (1990).

22. Meents, A., Gutmann, S., Wagner, A. & Schulze-Briese, C. *Proceedings of the National Academy of Sciences of the United States of America* **107**, 1094-1099 (2010).

23. Larsen, F.K. *Acta Crystallogr B* **51**, 468-482 (1995).

24. Chen, V.B. et al. *Acta crystallogr D* **66**, 12-21 (2010).

25. Schindelin, J. et al. *Nat Methods* **9**, 676-682 (2012).